Soft Matter

PAPER

View Article Online
View Journal

Cite this: DOI: 10.1039/c8sm02625d

Diffusion-limited dissolution of calcium carbonate in a hydrogel

Alexandre Turani-i-Belloto, Nathan Meunier, Paola Lopez and Jacques Leng *

Received 28th December 2018,
Accepted 2nd February 2019

DOI: 10.1039/c8sm02625d

rsc.li/soft-matter-journal

In the process of fabricating porous polymers, we use dispersed calcite as a sacrificial solid that generates porosity after dissolution. To do this, we trap calcite particles in a hydrogel, dissolve the particles and dry the hydrogel; here, we describe in detail the dissolution kinetics. We prepare PEGDA [poly(ethylene glycol)-diacrylate] water solutions loaded with micron-sized calcite particles (containing mostly calcium carbonate) up to about 30% volume fraction; these dispersions are photo-polymerized into hydrogels as flat and shallow monoliths with a typical thickness of ≈100 μm and a lateral extent on the order of 1 cm. These soft hydrogels are then soaked into an acidic solution (HCl) which induces the dissolution of the carbonates. The dissolution fronts remain sharp throughout the dissolution and progress inward in a diffusive manner. Such a kinetics is well described numerically using a mean-field diffusion–reaction model where the diffusion of the acid strongly limits the process.

1 Introduction

The dissolution kinetics of carbonates is an important issue in fields such as geology,[1] water remediation,[2] desulfurization,[3,4] oil recovery,[5,6] leaching or carbonation of concrete/cement,[7] *etc.* In most of these processes, the crucial point is obviously how the mineral (limestone, calcite, containing mostly $CaCO_3$, *etc.*) is contacted with an acidic solution; the subsequent dissolution kinetics involves many different stages, sometimes limited by the chemistry of secondary reactions,[8,9] most often limited by the transport of reactants and products.

Calcite is one of the minerals that dissolves the quickest[9–11] in moderate to strongly acidic solutions. While in most situations transport and reaction are intimately mixed,[8] high dissolution rates explain why it is sometimes difficult to find conditions in which transport of solutes and reactants does not impede the dissolution kinetics. Here, we deliberately force the transport of all the solutes and reactants but the carbonate to be diffusive: we trap micron-sized calcium carbonate particles in a dense hydrogel and soak the composite hydrogel in a strong acid. The dissolution proceeds from the exposed faces of the gel and progresses inward to 1. We observe sharp dissolution fronts that progress in depth (Fig. 2d and e). This observation is reminiscent of the pioneering work of Léger and coworkers[12] where a sharp corrosion front occurs in a porous medium upon diffusion of reactants, a situation which was soon finely theorized by Bazant and Stone.[13] Our composite hydrogel falls reasonably well in their description of one diffusing species (the acid) reacting with a static one (the mineral); unlike ref. 13, we study here finite-size samples for which we do not expect to extract asymptotic regimes.

Specifically, we investigate systematically the impact of experimental parameters such as the concentrations of acid and carbonate on the dissolution kinetics and we find that it follows a simple law: the dissolution is frontal, that is, the front always remains perfectly flat and sharp and progresses inward in a diffusive manner ($z_f \sim \sqrt{t}$). Using a numerical mean-field reaction–diffusion scheme, we confirm that such a diffusion-limited kinetics is a natural consequence of the high dissolution rate of calcite combined with a slow diffusion of the acid in the gel. It permits us to analyze quantitatively our experiments and to suggest that the hydrogel composite matrix represents a

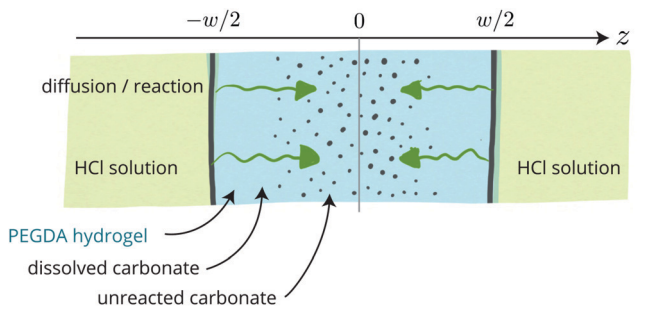

Fig. 1 (side view) Geometry of a hydrogel slab of thickness w (in blue), initially loaded with trapped calcium carbonate microparticles at volume fraction ϕ, and plunged into an acid bath (HCl, in green) kept under magnetic stirring. The acid diffuses into the hydrogel leading to the dissolution of the carbonate particles.

University of Bordeaux, Laboratory of the Future (CNRS/SOLVAY), 178, avenue du Docteur Schweitzer, 33600 Pessac, France. E-mail: jacques.leng-exterieur@solvay.com; Fax: +33 5 56 46 47 99; Tel: +33 5 56 46 47 49

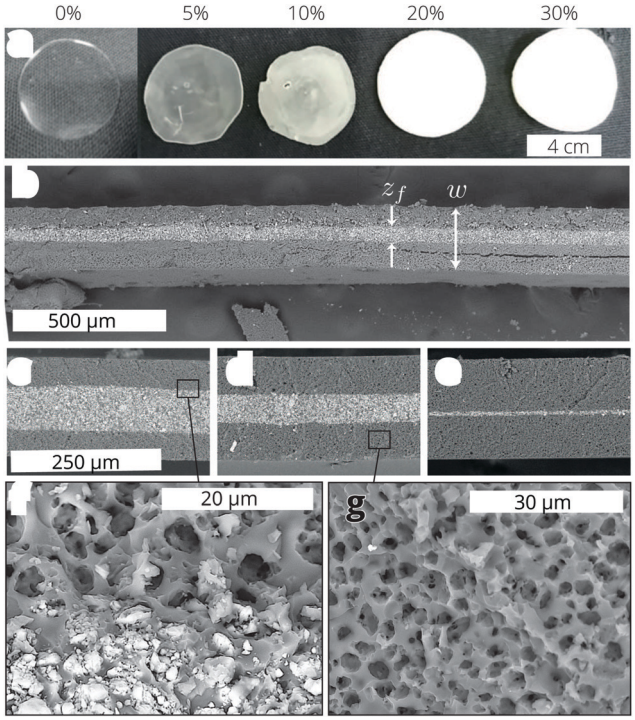

Fig. 2 (a) Top view of the monoliths prepared with different volume fractions of calcite (upper label), after photo-polymerization, dissolution and drying. (b–g) Typical SEM observations of the partial dissolution of the carbonate particles (showing in white) trapped in the middle of the polymer slab: (b) side-view of the slab highlighting a sharp dissolution front, z_f, initiated from the face; (c–e) time evolution of the dissolution front progressing in depth yet retaining a sharp nature; (f) closer view at the level of the dissolution front and (g) in the dissolved part evidencing the porous nature of the polymer, here with a volume fraction of voids of 30%.

simple, versatile and possibly useful system for diffusion-limited reactions often encountered with quiescent fluids or porous media.

Eventually, the full dissolution of the sacrificial porogenic carbonate[14,15] leads to a porous polymeric structure (Fig. 2g) whose porosity is isometric to the initial particles, both in volume fraction and in size.

2 Experimental methods

2.1 Chemicals and formulation

The core of the formulation contains a mixture of an oligomer [PEGDA, poly(ethylene glycol)-diacrylate, M_n = 700 g mol^{-1}, density $\rho = 1.12 \times 10^3$ kg m^{-3}, Sigma-Aldrich], a photo-initiator [HMP, 2-hydroxy-2-methylpropiophenone, $M_w \approx 164.02$ g mol^{-1}, density $\rho = 1.077 \times 10^3$ kg m^{-3}, Sigma-Aldrich, also known as Darocur 1173] and ultra-pure water (W) in mass proportions PEGDA : W : HMP 1 : 1 : 0.15. We add calcite particles (C, bare micronized calcite, Microcarb 60, kindly offered by Reverté Productos Minerales;† volume-averaged diameter of ≈1.3 μm distributed between 0.2 and 10 μm, molar mass $M_w \approx 100.09$ g mol^{-1}, density $\rho = 2.71 \times 10^3$ kg m^{-3}) and a polyelectrolyte [PSS, poly(sodium 4-styrenesulfonate) $M_w = 70 \times 10^3$ g mol^{-1}, density $\rho = 0.8 \times 10^3$ kg m^{-3}, Sigma-Aldrich] at mass ratio C : PSS 30 : 1 which was optimized empirically (PSS is a common stabilizer of $CaCO_3$[16] which prevents aggregation of particles and in turn retards sedimentation). The final volume fraction of calcite varies between ϕ = 5 and 30% and is calculated from the weights and densities of all constituents assuming an ideal mixing rule. Eventually, the calcite is dissolved in acidic solutions prepared by diluting a 2 M HCl stock solution (from VWR) with ultra-pure water.

† This natural calcite contains 98.96% $CaCO_3$ (mass fraction), 0.59% $MgCO_3$, 0.12% SiO_2, 0.045% Al_2O_3, 0.044% Fe_2O_3, and traces of metals.

2.2 Fabrication of thin monoliths of carbonate-loaded PEGDA hydrogels

About 0.3 mL of the formulation is pipetted and squeezed in between two glass slides (thickness 1 mm) spaced with a 280 μm-thick silicone washer in all experiments conducted here. It is then exposed to ultra-violet radiation for a time period of δt using a collimated LED working at 365 nm (a UV-KUB1 from Kloé delivering a tunable power density up to $I \approx 500$ W m^{-2}). The dose $I\delta t$ required to fully polymerize the slab depends mostly on the amount of photo-initiator, the carbonate load, the dissolved oxygen, the thickness of the slab, *etc.*, and has to be calibrated.[17,18] A dose of 500 J m^{-2} is sufficient here for the most concentrated sample and we post-process the slab by curing it from the two faces in order to ensure a symmetrical sample with possibly a homogeneous conversion throughout its thickness. This procedure yields a thin and shallow hydrogel which turns from transparent to whitish to opaque as the carbonate load is increased (Fig. 2a).

The structure of the hydrogel has been described in many papers, see for instance the work of De Molina & Co[19] and references therein. To make it simple, for thin samples with no particles the kinetics of photo-polymerization of acrylates happens in 3 dimensions everywhere in space, and is strongly dependent on the photo-initiator *via* its concentration and reactivity. We end up with a 3D gel where cross-links are due to acrylate polymers of a length which is hard to quantify. Depending also on the UV dose, the number of cross-links may vary. Therefore, there are in principle many degrees of freedom to tune the property of the gel. Besides, these gels are not known to be pH-dependent except for their long term stability and degradation in acidic media.[20]

2.3 Dissolution *via* wet etching

We first soak the thin slab in ultra-pure water for 15 minutes in order to fully swell the hydrogel and to get rid of traces of the unreacted photo-initiator; indeed, we found that it yields the best reproducibility as it probably permits us to bypass some issues related to the partial drying of the gel. Then, we plunge the composite hydrogel into a bath of a hydrochloric acid solution at known concentration and for a given incubation time, kept under magnetic stirring. The bath has a very large volume (∼50 mL) as compared to that of the slab (<0.5 mL). We 3D-printed a holder for the slab in order to

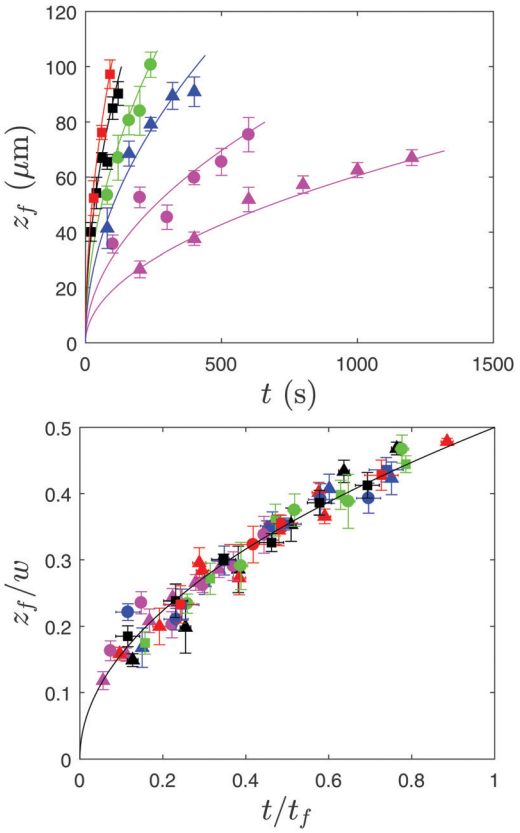

Fig. 3 Top: Dissolution front z_f of carbonates trapped in the gel against time t spent in the acidic bath for a selection of 6 conditions of acid concentration in the bath and carbonate concentration in the monolith (symbols indicate calcite concentrations and colors indicate HCl concentrations); the solid lines fit the data according to $z_f \sim t^{1/2}$. Bottom: Same data rescaled with the thickness of the monolith w and final dissolution time t_f; the solid line represents $z_f/w = 0.5(t/t_f)^{1/2}$.

minimize the mechanical stress exerted by the stirred fluid on the piece of gel and also to avoid buoyancy of the slab because of gaseous CO_2 production during the dissolution of the carbonate. Finally, the slab is extracted and thoroughly rinsed with ultra-pure water and left to dry under ambient conditions on a grid.

2.4 Analysis

In order to monitor how dissolution proceeds into the monolith, and more specifically the depth of dissolution $z_f(t)$, the monolith is cut and observed sidewise along the section using a scanning electron microscope (SEM tabletop TM3030Plus from Hitachi) after metal plating. A set of typical images is shown in Fig. 2. We studied the dissolution front as a function of the incubation time in the acid bath for a combination of 13 different concentrations of the acid and carbonate (among [HCl] = 0.06, 0.1, 0.25, 0.5, 0.75, 1 M and ϕ = 5, 10, 20, 30%). As it can be seen in Fig. 2b–f, the dissolution front is and remains sharp and its extent z_f can be unambiguously measured; its error is obtained by averaging typically 5 to 10 measurements. The dissolution time is also measured with an error of $\approx$10 s.

3 Experimental results

3.1 A diffusive dissolution kinetics

It seems clear from Fig. 2b–g that the dissolution kinetics proceeds *via* a reactive front which produces a very sharp dissolution interface. We measured the progression of this front as a function of the incubation time with a moderate temporal resolution—our SEM analysis technique being destructive—yet for a wealth of different concentrations of acid and carbonate and we evidence that the front progresses inward in a diffusive manner with $z_f(t) \sim t^{1/2}$.

Examples of this kinetics are given in Fig. 3 (top) where the plot of the front position against time is fitted with $z_f \sim t^{1/2}$. Rescaling the front positions with the monolith thickness w, we now define for every single condition the final dissolution time t_f estimated from the fit with $z_f(t_f)/w = 1/2$. The set of rescaled data z_f/w *versus* t/t_f is shown in Fig. 3, bottom, with a neat collapse of all conditions on the master curve $z_f/w = 0.5(t/t_f)^{1/2}$.

Out of these experiments, we thus extract the final-dissolution time t_f as a function of acid and carbonate concentrations. We use the ratio of concentrations $\mathscr{R} = [A]_r/[C]_0$ where $[A]_r$ and $[C]_0$ stand for the acid concentration in the reservoir and the initial carbonate concentration in the hydrogel (units of $M \equiv$ mol L^{-1}), respectively. We also use the diffusion time $\tau_D = w^2/D$ to scale the time, with D being the diffusivity of acid in the hydrogel. Here, $\mathscr{R}$ varies in the range of 10^{-2}–10^{0} and impacts the kinetics in a straightforward manner: $t_f \sim 1/\mathscr{R}$ as shown in Fig. 4. In order to match the model which we will describe next and which suggests that $t_f/\tau_D = 1/(4\mathscr{R})$, we tune D and obtain $D = 2.5 \times 10^{-10}$ m^2 s^{-1}.

We should state that all measurements were performed on a dry sample with SEM whereas experiments were performed in a wet state. On the one hand, the sample has skrunk due to drying ($w \approx 230$ μm), on the other hand, the sample was swollen in water ($w \approx 280$ μm). Therefore, we can rescale the

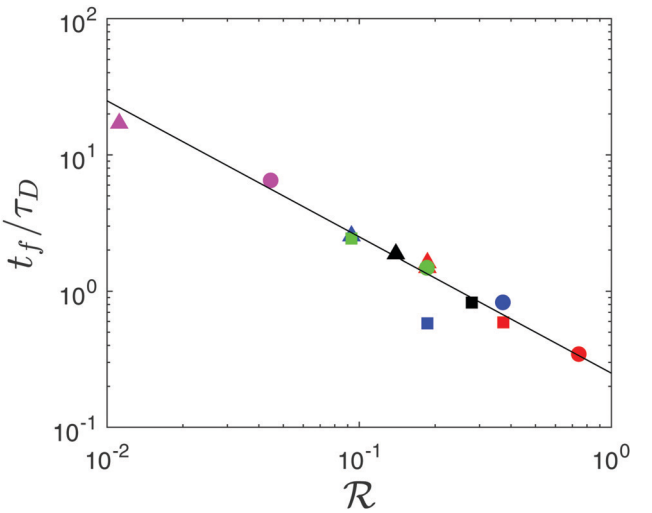

Fig. 4 Top: Dissolution time rescaled with the diffusion time of acid $\tau_D = w^2/D$ where $D = 2.5 \times 10^{-10}$ m^2 s^{-1} and $w = 230$ μm, the mean value of thickness of all dried samples; the solid line represents $t_f/\tau_D = 1/(4\mathscr{R})$ where $\mathscr{R}$ is the ratio of concentrations of acid in the bath over the initial concentration of carbonate in the hydrogel.

apparent diffusion coefficient with the swelling ratio: $D_{wet} = D_{dry}(w_{wet}/w_{dry})$ and we obtain now $D \approx 3 \times 10^{-10}$ m^2 s^{-1}.

4 A diffusion–reaction model

4.1 Geometry and model

Fig. 1 illustrates a cross section of the slab geometry, which reduces all transport phenomena to a uni-dimensional (1D) problem along the z direction normal to the faces of the slab, mainly because the slab is much thinner than wide (Fig. 2a and b).

In such configuration, the acid diffuses into the hydrogel from the faces of the slab and reacts with the trapped carbonate particles which leads to their dissolution though the overall reaction

$$CaCO_3 + 2HCl \rightarrow CO_2 + H_2O + CaCl_2,$$

where the particulate aspect of the carbonate does not come into account. The reaction actually lumps a set of subreactions involving carbonic acid, carbonate ions, *etc.*, which may actually control the kinetics depending on the pH, temperature, dissolved CO_2, *etc.* Under the conditions of a strong acid at fairly high concentration, the above-mentioned reaction is fast and irreversible[9] and encompasses correctly the main steps of the dissolution.

For the sake of the physical model, we rewrite the chemical equation as

$$C + 2A \rightarrow G + W + S, \quad (1)$$

where C stands for calcite or calcium carbonate, A for acid, G for gas, W for water, and S for salt.

Because the volume of the hydrogel slab is small ($\approx$0.3 mL) as compared to the volume of the acid solution in the bath ($\approx$50 mL), the acid that diffuses into the slab does not significantly alter the concentration in the bath; the latter solution being kept under stirring, we assume that the concentration in the bath and especially at the sides of the slab remains known and constant, namely $[A]_r$.

4.2 Reaction–diffusion equations

The acid progresses in the hydrogel through some molecular diffusion process with a diffusion coefficient D whereas we consider that the carbonate particles are trapped in the mesh of the hydrogel ($\sim$ 5–10 nm[19]) and do not diffuse. The set of coupled diffusion–reaction equations thus reads as:

$$\frac{\partial[A]}{\partial t} = D\frac{\partial^2[A]}{\partial z^2} - 2\Gamma, \quad (2)$$

$$\frac{\partial[C]}{\partial t} = -\Gamma, \quad (3)$$

where Γ is the rate at which acid and carbonate are consumed upon dissolution (units of M s^{-1}) and is defined as: $\Gamma = -\frac{d[C]}{dt} = -\frac{1}{2}\frac{d[A]}{dt}$ from the stoichiometric coefficients [eqn (1)]. The boundary conditions (BCs) are the following: the acid concentration in the bath is constant everywhere in space and time and specifically at the edge of the slab: $[A(z = -w/2,t)] = [A(z = w/2,t)] = [A]_r$, whatever the time t. The initial conditions (ICs) are: no acid in the slab to start with: $[A(-w/2 < z < w/2, t = 0)] = 0$ and a constant and homogeneous

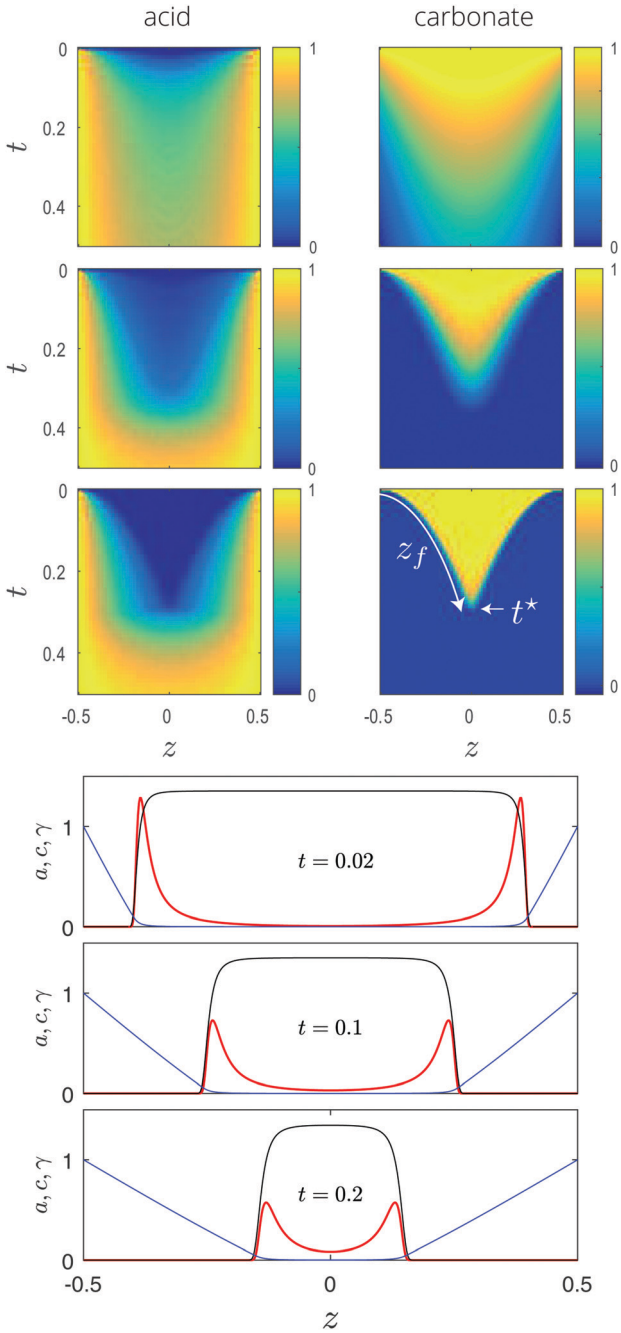

Fig. 5 Top: Concentration maps in the slab of acid (left) and carbonate (right) in reduced units a, c, t, and z for several Damköhler numbers (10^1, 10^3, 10^5 from top to bottom) for a ratio of concentrations $\mathscr{R} = 1$. Highlighted on the bottom right plot is the trajectory of the dissolution front $z_f(t)$ and the final dissolution time $t^\star$. Bottom: An example of the concentration profiles of the acid (a, blue), the carbonate (c, black) and the reaction rate (γ, red, scaled by a factor of 1/2500 everywhere) across the slab at several times for a partial order of reaction $m = 2$ [Da = 2×10^5, $a_r(0) = 1$, $c_0(0) = 1.3538$, $\mathscr{R} = 0.7387$, $t^\star = 0.3825$].

initial concentration of carbonate in the slab: $[\mathrm{C}(-w/2 < z < w/2, t = 0)] = [\mathrm{C}]_0$ (and no carbonate in the bath).

4.3 Reaction scheme

Consistent with literature results and for the sake of simplicity, we adopt the fairly general form $\Gamma = k[\mathrm{A}]^m[\mathrm{C}]^n$ where k is the rate constant of the reaction [units of $\mathrm{M}^{-(m+n-1)}$ s^{-1}]. It is believed that for the carbonate the reaction is of partial order $n = 1$;[9] for the acid however, m has been measured between 1 and 2, including non integer values (*e.g.* $m = 1.643$ in the most recent results[9]). We thus keep $\Gamma = k[\mathrm{A}]^m[\mathrm{C}]$ with $1 \leq m \leq 2$ for our numerical description.

We now turn to unitless variables. Space is scaled with w: $z \rightarrow z/w$, time with the diffusion time $\tau_\mathrm{D} = w^2/D$ of acid across the slab $t \rightarrow t/\tau_\mathrm{D}$ (D is the diffusion coefficient of acid in the hydrogel), and all concentrations are scaled with that of the acid in the bath $[\mathrm{A}]_r$, thus $[\mathrm{A}] \rightarrow a \equiv [\mathrm{A}]/[\mathrm{A}]_r$ and the carbonate concentration $[\mathrm{C}] \rightarrow c \equiv [\mathrm{C}]/[\mathrm{A}]_r$. It should be noted that other unitless variables have been used in theoretical studies of diffusion–reactions in a semi-infinite medium;[13] in such a case however, there is no natural timescale for diffusion and normalization is performed using a typical timescale of the reaction. We find in our case that diffusion is more natural indeed and using the unitless variables given above, the equations read:

$$\frac{\partial a}{\partial t} = \frac{\partial^2 a}{\partial z^2} - 2\mathrm{Da} \times a^m \times c, \tag{4}$$

$$\frac{\partial c}{\partial t} = -\mathrm{Da} \times a^m \times c, \tag{5}$$

where $\mathrm{Da} = k[\mathrm{A}]_r^m\tau_\mathrm{D}$ is a Damköhler number comparing the timescale of diffusion τ_D to one related to the reaction $(k[\mathrm{A}]_r^m)^{-1}$. BCs read as $a(z = -1/2, t) = a(z = 1/2, t) = 1$, whereas t and ICs read as $a(-1/2 < z < 1/2, t = 0) = 0$ and $c(-1/2 < z < 1/2, t = 0) = 1/\mathscr{R}$ where $\mathscr{R} = [\mathrm{A}]_r/[\mathrm{C}]_0$ is the ratio of initial concentrations. Eventually, the rate of the reaction now reads as $\gamma \equiv \Gamma/([\mathrm{A}]_r/\tau_\mathrm{D}) = \mathrm{Da} \times a^m \times c$.

4.4 Numerical solutions

The previous equations are solved numerically (using the PDEPE package in MATLAB) with three parameters, the Damköhler number Da, the ratio of concentrations of acid-to-carbonate $\mathscr{R}$, and the partial order of the reaction m. In the regimes explored here ($\mathrm{Da} \geq 10$), the dissolution kinetics of the acid in the hydrogel turns from mixed (diffusion and reaction based) to fully diffusion-limited, and a clear effect can be seen upon increasing Da whereby the dissolution fronts become sharper (Fig. 5).

5 Numerical results and discussion

Within this mean-field numerical scheme, we observe that at high Da, the dissolution is frontal indeed and the fronts always follow a diffusive law with $z_\mathrm{f} \sim t^{1/2}$, already obvious on the cartography of acid, Fig. 5 ($\mathrm{Da} = 10^5$) and re-demonstrated in rescaled units as shown in Fig. 6, top. In practice, we actually fix a high Da value for one condition ($>10^5$, supported by an estimate given in Appendix A7.1) and solve consistently the numerics with respect to the experiments, recalling that Da depends on the concentration of acid: $\mathrm{Da} = k[\mathrm{A}]_r^m\tau_\mathrm{D}$; it is therefore compulsory to adapt it as a function of $[\mathrm{A}]_r$ and $[\mathrm{C}]_0$, which in turn modifies $\mathscr{R}$, one boundary condition.

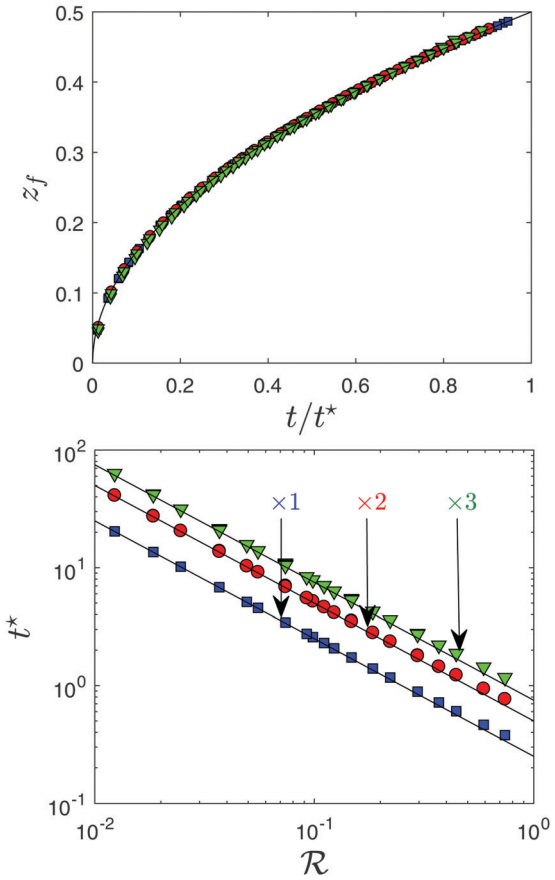

Fig. 6 Top: Rescaled dissolution fronts for a selection of ratios $\mathscr{R}$ and for the three partial orders of the reaction. Bottom: End-dissolution time t obtained from numerics and plotted against the ratio of concentration $\mathscr{R}$. The data have been scaled for clarity by a factor shown in the figure. The solid lines represent $t = 1/(4\mathscr{R})$ modulo the scaling factors. Same color coding for the two plots: the partial order of the reaction is $m = 1$ in blue, $m = 1.643$ in red, and $m = 2$ in green.

We extract the end-dissolution time $t^\star$ (Fig. 6, bottom) as a function $\mathscr{R}$ for the three orders m we studied. It should be noted that in these plots (Fig. 6 bottom), the points and solid lines have been shifted for clarity but they all actually stand on a single and unique curve. Within the numerical error of the analysis, which basically relies on image and profile analysis of data obtained from the maps as shown in Fig. 5, we find that whatever m,

$$t^* = \frac{1}{4\mathscr{R}}. \tag{6}$$

The agreement with experiments is qualitatively excellent and can even be made quantitative by tuning D in order to get $t^\star = t_\mathrm{f}/\tau_\mathrm{D}$, see Fig. 4.

We obtain $D \approx 2.5 \times 10^{-10}$ m^2 s^{-1}, a value which is unexpectedly low for the diffusivity of acid in the hydrogel,

especially when the mesh size of the gel is very large compared to the size of the hydronium ion. We thus measured it independently using a pH-sensitive dye (see Appendix A7.2) and the estimate we obtained is also fairly small, $D \approx 5 \times 10^{-10}$ m^2 s^{-1}. Such a low value may originate either from an interaction of the acid with the gel (see ref. 21 and references therein) or because the diffusivity is that of a pair of ions HCl^+–Cl^- instead,[22] as required to fulfill electro-neutrality.

We leave it as an open question which does not alter our main results: in a case where one reactant is static and captures eagerly the other diffusing species, the process is quite naturally limited by diffusion and the numerics also sustain that the details of the reaction are not accessible to the experiment (*i.e.*, results do not depend on Γ).

Such a result turns out to be particularly simple and we can predict any practical kinetics of frontal dissolution in real units with $z_f = (\mathscr{R}Dt)^{1/2}$, where D reflects some diffusivity of the acid in the hydrogel and which remains the only unknown parameter of the problem. Interestingly, our experiments turn out to be a measurement of D.

Importantly, numerics help us to rephrase the problem: we rewrite the present diffusion–reaction problem into a diffusion problem with a moving boundary, the reaction front. As the kinetics is fast, the position of the front z_f defines a 'sink' boundary condition equivalent to $a(z_f) \equiv 0$. We indeed observe in Fig. 5, bottom, that the acid falls linearly from its value at the edge of the slab to 0 at the level of the front. In real units, the scaling behavior now becomes obvious: the flux of acid is given by $j_A = -D[A]_r/z_f$, where every two moles of incoming acid is captured by the carbonate. After a delay of δt, a new length of carbonate δz_f is dissolved according to $(j_A/2)\delta t = [C]_0 \delta z_f$, from which we get $z_f^2 = \mathscr{R}Dt$, as observed numerically and experimentally.

6 Conclusions and perspectives

We observe that the dissolution of calcite particles trapped in a dense hydrogel proceeds here through a diffusion-limited mechanism. It was not obvious from the beginning as it requires the right imbalance between dissolution and diffusion and this regime breaks down when the Damköhler number is no longer very high. We show in Appendix A7.1 that this number can also be described using macroscopic observables such as the size of particles r_p, the dissolution rate κ, and the diffusion time: $Da \sim \kappa\tau_D/r_p$ which highlights the key ingredients for getting this regime. Most minerals dissolve much more slowly than calcite[11] and this is a key issue for the diffusion-limited regime. Calcite is therefore the perfect choice as a sacrificial solid; however, many other solids are interesting porogens but might not lead to such a specific diffusion-limited regime: they might as well dissolve homogeneously throughout the matrix to also end up with a porous matrix.

Beside, we evidence that in a diffusion-limited process, no details of the chemistry can be obtained by following the kinetics: the interwoven diffusion and reaction processes can however be significantly simplified and transformed into a diffusion process with a moving boundary condition, a sink that only accounts for the stoichiometry of the reaction. However, we monitor that the diffusivity of acid in the gel should not be taken as the one in bulk, an unexpected result.

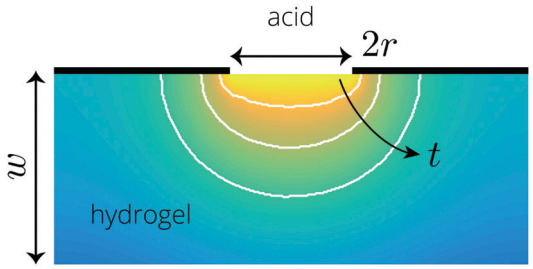

Fig. 7 Sketch of a guided dissolution through a mask.

The simplicity and accuracy with which we can describe the dissolution kinetics is suggestive of more complicated situations. Inspired by the elegant piece of work by Harris[23] coined 'evaporative lithography', where the diffusive process of evaporation is performed across a mask and leads to a structured deposit, we suggest to perform 'guided dissolution', as illustrated in Fig. 7. A hydrogel loaded with a mineral would be contacted with acid through a mask in order to limit spatially the contact and to set specific boundary conditions. We expect to maintain a diffusion-limited dissolution process and to be able to structure in volume the dissolution. In particular, if the size of the mask ($2r$) is smaller than w the thickness of the slab, we expect to observe a point-like source at $w^2 \gg \mathscr{R}Dt \gg r^2$, thus resulting in a dissolution taking place in a hemispherical cap, whereas the dissolution will be planar at the very early stage of the process. In addition, a periodic pattern of holes in the mask will lead to interesting dissolution patterns throughout the process.

It could also be interesting to study the reverse process of diffusion-limited precipitation where a slab first soaked with a salt would be contacted with another salt. The macro-porous gel would serve as a template for precipitation[24] of the new species. Now, if the hydrogel is initially partially dissolved using the first mineral, we will obtain a super-structure combining the two minerals.

Guiding the dissolution, the (re)precipitation, and also using, for instance, microfluidics for shaping new templates for the hydrogel[25] could add interesting and hierarchical levels of complexity in the morphologies we wish to engineer.

Conflicts of interest

There are no conflicts to declare.

A Appendix

A.1 Estimating the chemical rate

We can obtain values of dissolution rates of calcite in the literature but these values are quite scattered.[9–11] For the sake

of order of magnitude only, we extrapolate the range $\kappa = 10^{-2}$–1 mol m^{-2} s^{-1} for [HCl] = 1 M.

If we assume a monodispersed suspension of calcite particles of radius r_p and volume fraction ϕ in a volume sample V, dimensional analysis leads us to a reaction rate Γ from the total surface of particles S_p: $\Gamma = S_p\kappa/V = 3\kappa\phi/r_p$. Typical values of calcite reaction rates therefore range from $\Gamma = 1.5 \times 10^3$–9×10^5 M s^{-1}.

For simplicity, we chose here a partial second order reaction $\Gamma = k[A]^2[C]$ which therefore yields $k = 3\kappa\phi/(r_p[A]^2[C])$. With $[C] = 10^{-3}\rho\phi/M_w$ where [C] is in units of mol L^{-1}, ρ the density of calcite (2.71×10^3 kg m^{-3}) and M_w its molar mass (100.09×10^{-3} kg mol^{-1}), we end up with $k = 3 \times 10^3\, M_w\kappa/(\rho[A]^2 r_p)$. We can thus get a lower bound for the Damköhler number in relation to our experiments: $Da \approx 3 \times 10^3 M_w\kappa\tau_D/(\rho r_p) \approx 2 \times 10^5$, which confirms the diffusion-limited aspect of the process.

A.2 Imaging the diffusion in hydrogels

We estimate the diffusivity of several species within the hydrogel. To do so, we prepare a large, flat and roughly cylindrical piece of water-saturated hydrogel (thickness ≈ 280 μm, diameter ≈ 8 mm), macro-porous or not, which we squeeze in between two glass slides of large dimensions. Importantly, in all cases where macro-porosity is mentioned, it results from the preliminary and full dissolution of calcite particles. Then, the slab is contacted with a colored or acidic solution, and a diffusion process occurs in a radial manner starting from the edge of the slab. Two situations were studied:

– we put a 'passive' dye in the external solution, here Acid Blue 9 in water (M_w = 783 g mol^{-1}, density $\rho \approx 1.2$ g cm^{-3}, used at about 1 mM), which will diffuse into the hydrogel, see Fig. 8 top;

– we put a 1 M HCl solution around a slab that was previously soaked with a pH-sensitive dye overnight (methyl orange M_w = 327.33 g mol^{-1} at a concentration of 1 mM, pK_a = 3.47, the color change at pH = 3–4), as shown in Fig. 8 bottom.

In both cases, color changes are recorded using a reflex digital camera at a rate of about 0.1–1 frame per minute. When the slab is porous, imaging is more complicated, very often performed with a backlight, and sometimes impossible due to strong light scattering.

These experiments are analyzed on the basis of the spatio-temporal solution of the diffusion equation in the cylindrical geometry of a species diffusing radially with some diffusion coefficient D and where the concentration is kept constant at the edge R_0 of the slab. The diffusivity D of the species is used as the only free parameter to fit the experimental data.

For the blue dye (Fig. 8 top), we set the front position at $c_0/2$ where c_0 is the concentration at the edge of the slab, and we obtain an estimate of the molecular diffusion coefficient $D = (9.2 \pm 2.2) \times 10^{-10}$ m^2 s^{-1} which is consistent with the diffusion coefficient of a freely moving molecule in water. Here, the gel phase does not seem to play a significant role in the diffusion process.

The measurement of the diffusion coefficient of the acid is much less direct. In the experiments, the acid diffuses into a slab of gel which was soaked with methyl orange; when the concentration of acid increases above a given threshold, pH ≈ 3–4, the color indeed changes. A proper model would couple diffusion of two species (the acid and pH-sensitive dye)

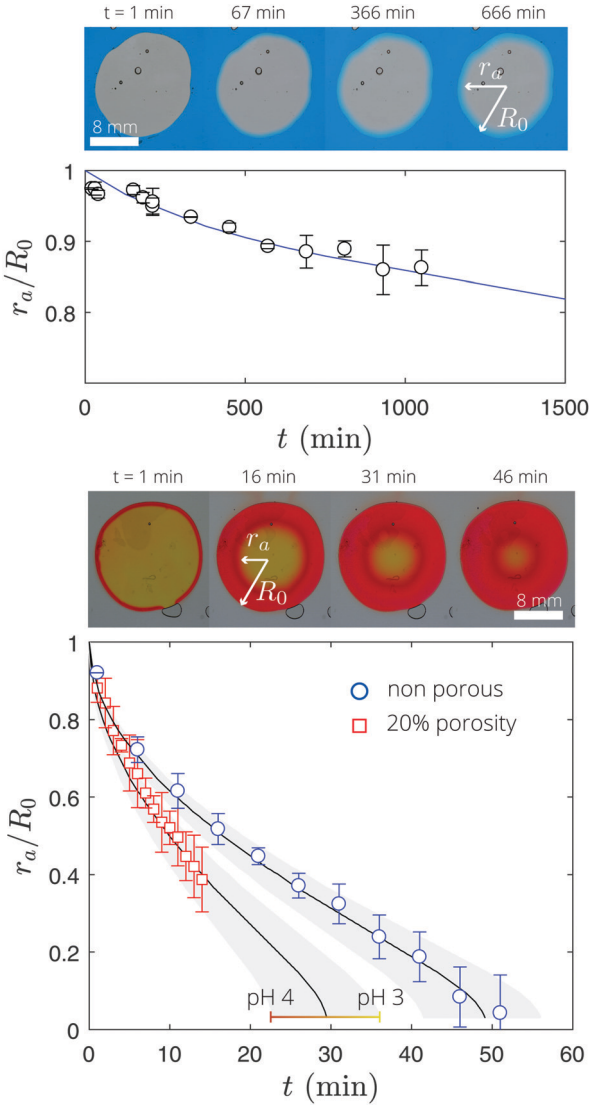

Fig. 8 Top: Inward diffusion of a blue dye where the color front (r_a from the center of a slab of radius R_0) is followed by image analysis against time. The line is the theoretical prediction of the concentration front (actually where $c(r_a,t) = c(R_0)/2$) which permits us to extract the estimate of diffusion of the dye in the hydrogel. Bottom: The same type of experiment where the color front shows the change of state of the pH sensitive dye (in the range of 3–4). In this example, the outer acid concentration [HCl] = 1 M and plain or porous hydrogels have been studied. The solid lines represent here the concentration at an average pH = 3.4 and the shaded regions show the range of pH = 3–4 where the dye changes color. Here, the images are obtained for a plain hydrogel, which displays the best contrast.

with the corresponding acid–base reaction of the weak acid (the dye) with hydronium ions. As a gross simplification, we first assume that the dye does not diffuse at all; then, we neglect the chemical reaction and state that the kinetics is instantaneous at pH ≈ 3–4. In practice, we tune D in order to fit the color front position with two limits we calculate at pH = 3 and pH = 4 (see the gray zone in Fig. 8, bottom). We acknowledge that this procedure is quite naive, but it is used here mostly to investigate the effect of the pure-water zone (water cavities) in the hydrogel due to the former calcite particles. We extract

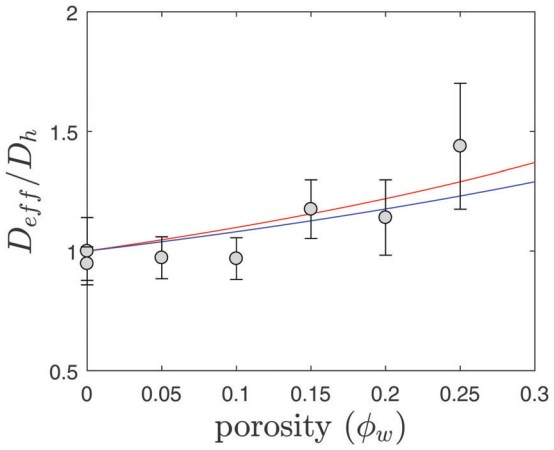

Fig. 9 Diffusion coefficient of H_3O^+ relative to the one in the plain hydrogel against the volume of water cavities, ϕ_w. Gray represnts the measured values using the pH-sensitive dye, and the solid line shows the basic model, see text, with $D_h = 5 \times 10^{-10}$ m^2 s^{-1} and $D_w = 5 \times 10^{-9}$ m^2 s^{-1} (in red) or $D_w = 2 \times 10^{-9}$ m^2 s^{-1} (in blue).

$D = (5.6 \pm 0.2) \times 10^{-10}$ m^2 s^{-1} in the case of a plain hydrogel and up to $D = (8.2 \pm 1.5) \times 10^{-10}$ m^2 s^{-1} with 25% volume of water cavities in the hydrogel (Fig. 9).

We find that the diffusivity of the acid in the plain hydrogel is very low, and actually comparable to the one of the dye; one of our approximations thus clearly breaks down. While we implemented the reaction–diffusion problem with two diffusing species, we found that the actual solution depends on too many unknown parameters and is thus not reliable.

We also found that the diffusion coefficient of the acid depends very little on the existence of water cavities with a volume fraction ϕ_w in the hydrogel which is actually calculated directly using the volume fraction of sacrificial calcite particles used in the formulation. Basically, effective diffusivity D_{eff} can be described as a volume average of diffusivity into water zones (diffusivity D_w, volume fraction ϕ_w) and into hydrogel zones (diffusivity D_h, volume fraction $\phi_h = 1 - \phi_w$) according to: $D_{eff}^{-1} = \phi_w D_w^{-1} + \phi_h D_h^{-1}$. Fig. 9 indeed confirms such a trend.

To conclude, we will neglect in the first approximation the effect of pure water cavities in the diffusion–reaction dissolution kinetics and somehow confirm that the diffusivity of the acid in the hydrogel is of the order of 10^{-10} m^2 s^{-1}.

Acknowledgements

We are grateful to Jean-Baptiste Salmon, Flavie Sarrazin, and Fabienne Gauffre for help and useful comments. We thank Mr Xavier Zaballos, export manager at S. A. Reverte Productos Minerales for supplying us with calcium carbonate samples used in the present study.

Notes and references

1 J. W. Morse, R. S. Arvidson and A. Lüttge, *Chem. Rev.*, 2007, **107**, 342–381.
2 M. Lee, I. S. Paik, I. Kim, H. Kang and S. Lee, *J. Hazard. Mater.*, 2007, **144**, 208–214.
3 M. Kawase and M. Otaka, *Waste Management*, 2013, **33**, 2706–2712.
4 R. A. Pandey, R. Biswas, T. Chakrabarti and S. Devotta, *Crit. Rev. Environ. Sci. Technol.*, 2005, **35**, 571–622.
5 G. Daccord, R. Lenormand and O. Liétard, *Chem. Eng. Sci.*, 1993, **48**, 169–178.
6 M. Ghommem, W. Zhao, S. Dyer, X. Qiu and D. Brady, *J. Pet. Sci. Eng.*, 2015, **131**, 18–33.
7 M. Mainguy, C. Tognazzi, J. M. Torrenti and F. Adenot, *Cem. Concr. Res.*, 2000, **30**, 83–90.
8 C. N. Fredd and H. S. Fogler, *Chem. Eng. Sci.*, 1998, **53**, 3863–3874.
9 C. Carletti, H. Grénman, C. De Blasio, E. Mäkilä, J. Salonen, D. Y. Murzin, T. Salmi and T. Westerlund, *J. Chem. Technol. Biotechnol.*, 2015, **91**, 1517–1531.
10 R. S. Arvidson, I. E. Ertan, J. E. Amonette and A. Luttge, *Geochim. Cosmochim. Acta*, 2003, **67**, 1623–1634.
11 J. D. Rimstidt, *Appl. Geochem.*, 2015, **61**, 99–108.
12 C. Léger, F. Argoul and M. Z. Bazant, *J. Phys. Chem. B*, 1999, **103**, 5841–5851.
13 M. Z. Bazant and H. A. Stone, *Phys. D*, 2000, **147**, 95–121.
14 L. Wu, S. Bai and Y. Sun, *Biotechnol. Prog.*, 2003, **19**, 1300–1306.
15 M. Mehraban, A. Zadhoush, S. Abdolkarim Hosseini Ravandi, R. Bagheri and A. Heidarkhan Tehrani, *J. Appl. Polym. Sci.*, 2013, **128**, 926–933.
16 C. Wang, C. He, Z. Tong, X. Liu, B. Ren and F. Zeng, *Int. J. Pharm.*, 2006, **308**, 160–167.
17 A. Vitale, M. G. Hennessy, O. K. Matar and J. T. Cabral, *Adv. Mater.*, 2015, **27**, 6118–6124.
18 K. C. Wu, K. F. Seefeldt, M. J. Solomon and J. W. Halloran, *J. Appl. Phys.*, 2005, **98**, 0249902.
19 P. M. De Molina, S. Lad and M. E. Helgeson, *Macromolecules*, 2015, **48**, 5402–5411.
20 M. B. Browning, S. N. Cereceres, P. T. Luong and E. M. Cosgriff-Hernandez, *J. Biomed. Mater. Res., Part A*, 2014, **102**, 4244–4251.
21 B. Penke, S. Kinsey, S. J. Gibbs, T. S. Moerland and B. R. Locke, *J. Magn. Reson.*, 1998, **132**, 240–254.
22 B. Abécassis, C. Cottin-Bizonne, C. Ybert, A. Ajdari and L. Bocquet, *New J. Phys.*, 2009, **11**, 075022.
23 D. J. Harris, H. Hu, J. C. Conrad and J. A. Lewis, *Phys. Rev. Lett.*, 2007, **98**, 148301.
24 J. Zhou, M. Zhou and R. A. Caruso, *Langmuir*, 2006, **22**, 3332–3336.
25 M. T. Gokmen and F. E. Du Prez, *Prog. Polym. Sci.*, 2012, **37**, 365–405.

